Journal of Power Sources 605 (2024) 234506

Contents lists available at ScienceDirect

Journal of Power Sources

journal homepage: www.elsevier.com/locate/jpowsour

Significance of *in situ* X-ray tomography for analysing buried interfaces in solid-state batteries: A case study on a Li/Li symmetric cell with a polymer-based electrolyte

Srabani Patra [a,b], Julien Morey [c], Lénaïc Madec [c,d], Peter Moonen [a,b,*]

[a] Université de Pau et des Pays de l'Adour, E2S UPPA, CNRS, DMEX, Pau, France
[b] Université de Pau et des Pays de l'Adour, E2S UPPA, CNRS, LFCR, Pau, France
[c] Université de Pau et des Pays de l'Adour, E2S UPPA, CNRS, IPREM, Pau, France
[d] Réseau sur le Stockage Electrochimique de l'Energie, CNRS FR3459, Amiens, France

HIGHLIGHTS

- *In situ* X-ray tomography for comprehending lithium-metal battery failure scenarios.
- 3D tomogram reveals polymer electrolyte thickening, puncturing and contact loss.
- Resistance measurements consistent with contact loss and subsequent cell shorting.
- *Ex situ* XPS identifies Li salts and organic compounds as source for thickening.
- *Ex situ* SEM confirms contact loss and presence of Li salts and organic compounds.

GRAPHICAL ABSTRACT

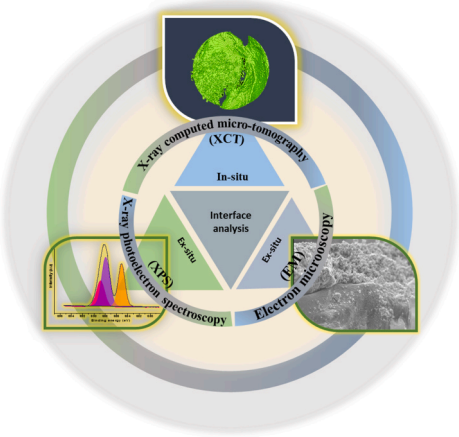

ARTICLE INFO

Keywords:
Buried interfaces
In situ X-ray tomography
Li/Li symmetric cell
Cell failure

ABSTRACT

Advanced *in-situ* characterization methods are crucial for comprehending how solid-state batteries evolve during cell cycling and to identify responsible factors for cell failure. In this study, we advocate for the use of laboratory-based *in-situ* X-ray tomography as a screening technique to non-invasively monitor the structural evolution of the cell of interest. The detected features of interest can be subsequently analysed by spectroscopic, microscopic and spectrometric techniques. To illustrate the proposed approach, we study the evolution of a Li symmetric cell while cycling from the pristine state up to cell failure. Pre-screening with *in-situ* X-ray tomography provides 3D images of the interface and suggests the occurrence of electrolyte thickening, puncturing and contact loss. These observations are consistent with impedance measurements conducted while cycling. Post-mortem XPS-analysis identifies lithium salt and organic compound accumulation on the electrolyte after cycling, providing a possible

* Corresponding author. Université de Pau et des Pays de l'Adour, Avenue de l'université, BP1155, 64013 Pau, France.
E-mail address: peter.moonen@univ-pau.fr (P. Moonen).

https://doi.org/10.1016/j.jpowsour.2024.234506
Received 18 January 2024; Received in revised form 11 March 2024; Accepted 4 April 2024
Available online 17 April 2024

explanation for the observed electrolyte thickness increment. SEM images give visual proof of the interfacial contact loss, and Auger mapping gives further confirmation of the XPS data. This case study illustrates that pre-screening using laboratory-based *in-situ* X-ray tomography, combined with in-depth analysis techniques, helps to advance our understanding of buried interfaces in solid-state batteries and to identify responsible factors for cell failure.

1. Introduction

The implementation of renewable energy resources critically relies on the development of energy storage systems. Among the various energy storage systems, solid-state batteries with a lithium metal anode have gained popularity due to their potential to improve safety and their high energy density. Therefore, solid-state lithium batteries can potentially be used for grid energy storage, and for other applications where reliable, long-lasting energy storage is needed [1–3].

Nowadays, most solid-state batteries are based on solid polymer electrolytes, as they present low flammability, flexible processability, and increased tolerance to vibration, shock, and mechanical deformation compared to liquid electrolytes [4–6]. However, the development of polymer-based solid-state lithium batteries is hindered by interfacial challenges such as passivating layer formation, lithium dendrite infiltration and limited ionic conductivity [7–10]. In order to improve the conductivity and enhance the interfacial contact, plasticizers are utilized in the polymer electrolyte, as seen in most commercial applications [11,12]. Despite this, the performance optimisation of polymer electrolytes is still regarded as a challenge.

A deeper understanding of the interface chemistry and possible failure scenarios is essential for ensuring ideal battery performance. As the behaviour at the interface is complex, a combination of complementary analysis strategies is required. Ideally, a typical laboratory workflow would start by preparing cross sections of the solid-state battery stack that are subsequently analysed by spectroscopic, microscopic and spectrometric techniques. Note, however that in the case of polymer-based solid-state batteries, the cross-section approach has only been proposed very recently [13,14]. The vast majority of the published studies are performed *ex situ*, although *in situ/operando* (S)TEM, ToF-SIMS and sXAS studies have been reported as well [13,14] and are rapidly gaining popularity. *In situ/operando* X-ray tomography studies of solid-state batteries have also been published [15–19]. As highlighted in Ref. [20], this technique enables advancing our understanding in three domains, namely (i) the relationship between structure and performance, (ii) the system dynamics, and (iii) the mechanical and structural degradation.

Some exceptions aside [16], most *in situ/operando* X-ray tomography studies have been performed at synchrotron facilities, where the high brilliance of the synchrotron X-ray beam allows combining excellent spatial and temporal resolution. While the technique is often termed non-destructive, a few authors called for caution as potential beam-induced damage could skew the conclusions of the investigations [21,22]. They show that damage can range from mild modifications of the crystalline structure to artificial phase transitions, and that this essentially depends on the mingled actions of dose and dose rate. Similar concerns are expressed regarding XAS [23], SEM and TEM [24].

In the current study we advocate for the use of laboratory-based X-ray tomography, as a screening tool, compatible with and complementary to the existing workflows. While the lower brilliance of laboratory-based X-ray tubes imposes a more stringent upper bound on the practically attainable combination between spatial and temporal resolution, we will demonstrate that the results still enable advancing (i) the relationship between structure and performance, (ii) the system dynamics, and (iii) the mechanical and structural degradation. Moreover, the lower dose rate of laboratory X-ray tubes reduces the risk for radiation damage for a given dose. Provided that optimal acquisition parameters are chosen for the battery system of interest, we argue that these characteristics render laboratory X-ray tomography ideal as a screening technique, to be used in combination with other analytical techniques.

While X-ray tomography is applicable to both anodes and cathodes, with both liquid and solid electrolytes, we will focus on the example of a polymer-based lithium symmetric cell to illustrate our claim. The cell is subjected to cycling at different current densities up to failure. A combination of advanced characterisation techniques was utilized, including X-ray tomography as a screening technique, and X-ray photoelectron spectroscopy and scanning electron microscopy/Auger analysis to confirm and complete the findings. As we will demonstrate, this approach allows to identify the fundamental issues of the studied cell and to suggest the appropriate measures for addressing them.

2. Experimental section

2.1. Electrochemical performance monitoring

A ~20 μm thick poly(vinylidene fluoride-*co*-hexafluoropropylene)-based (PVDF-HFP) copolymer electrolyte with lithium bis(fluorosulfonyl)imide (LiFSI) and different plasticizers, provided by the company ARKEMA, was assembled as part of a Li/electrolyte/Li symmetric cell stack under the inert atmosphere of an argon-filled glove box. The exact composition of the electrolyte cannot be disclosed without ARKEMA's consent, yet has no impact on the conclusions of the current study.

The cell was mounted between two stainless steel plungers in a ¼″ PFA (perfluoroalkoxy) Swagelok fitting. This setup is compatible with electrochemical and *in situ* X-ray computed tomography examinations. The PFA fitting prevents contact with oxygen, provides rotational symmetry, and has low X-ray attenuation, as required for the *in situ* measurements. Pressure was applied on the plungers to ensure good contact between the polymer electrolyte and the thin strips of metallic lithium. The current collectors (plungers) were connected to a VMP3 potentiostat (Biologic, France), and the symmetric Li/Li cell was galvanostatically cycled at 70 °C at different current densities. Each cycle lasted for 1 h. Li stripping-plating started at 0.03 mA/cm^2 and stepped up progressively to higher current densities up to cell failure.

2.2. In situ X-ray tomography

The inner microstructure of the symmetric cell stack was non-invasively visualised before and after cycling by means of lab based X-ray tomography. A Zeiss Xradia Versa 510 XRM was used. For each tomogram, 801 projections of 504 x 504 px were collected over a 360° angular range, with an exposure time of 5 s per projection. The X-ray tube voltage and power were set to 50 kV and 4 W, respectively, to ensure adequate X-ray flux and a satisfactory signal-to-noise ratio. The resulting dose was estimated to be below 40 kGy per scan, which is one order of magnitude smaller than the threshold reported in Ref. [21], below which the authors of that study did not detect visible damage for a liquid-based Li-ion battery on a synchrotron beamline (i.e. with an estimated ~10^{10} times higher dose rate). The tomographic datasets were reconstructed to produce a 3-dimensional (3D) stack. The resulting voxel size was 4 μm. Specific regions of interest of the degraded cell stack were subsequently analysed at 2 μm per voxel without physically altering the sample. For these scans, the exposure time per projection was increased to 20 s and both the size and the amount of projections were reduced to 401 projections of 241 x 241 px. All other parameters

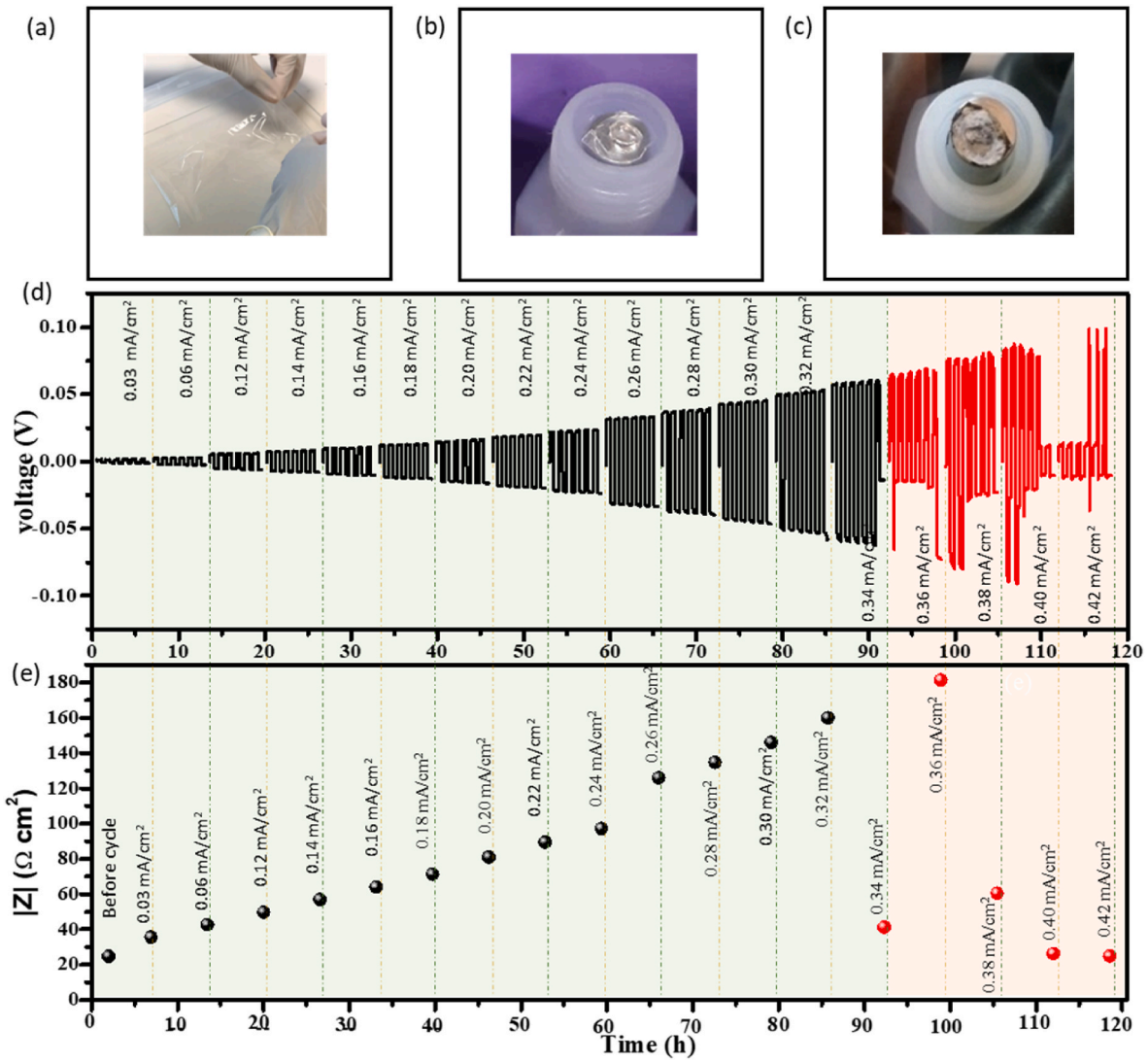

Fig. 1. (a) Image of the polymer electrolyte in a pristine state. Image of the polymer electrolyte in contact with lithium metal (b) before and (c) after cycling. (d) Voltage vs time pattern of Li/electrolyte/Li symmetric cell, 30 min of stripping/plating and (e) corresponding total resistance of the symmetric cell after cycling at each current density at 70 °C.

remained equal. After reconstruction, all 3D datasets were segmented into phases by means of the proprietary software package Dragonfly 2022.2 for Windows.

2.3. Pre and post cycling analysis

To corroborate the X-ray observations, *ex situ* XPS analysis was performed using an Escalab 250 Xi spectrometer with monochromatized Al Kα radiation (hν = 1486.6 eV). The pristine electrolyte polymer membrane and the cycled one (after cell disassembly under Ar and after lithium removal) were each placed on a sample holder using uPVC insulation tape (3 M part number 655) and then transferred into an argon-filled glove box connected to the spectrometer. To compensate for charging effects, the standard charge compensation mode was used with the same parameters for all samples. Core level spectra were recorded with a 0.15 eV step and a constant 20 eV pass energy using short-time iteration to follow any possible sample degradation. Homogeneity over the membrane surfaces was confirmed by performing three measurements on different areas for each sample. The binding energy scale was calibrated from the C–C/C–H peak at 285.0 eV using the CasaXPS software. Fitting was performed using either linear or Shirley-type backgrounds, 70 % Gaussian−30 % Lorentzian Voigt peak shapes and full width at half-maximum constraint ranges (same for all samples) to optimize areas and peak positions. XPS peak attribution was performed using reference samples available in the literature [25,26]. XPS quantification was performed using the relative sensitivity factor provided with the Escalab spectrometer.

To further support the findings, *ex situ* SEM/Auger analysis was performed on the interfacial region of the membrane after cycling using a JEOL JAMP 9500 F Auger spectrometer (JEOL Ltd, Tokyo, Japan). It was equipped with a Schottky Field Emission gun and a hemi-spherical analyser coupled with a high dynamic multichannel detector. The analysis was performed at 30–40° tilt to prevent the charging effect of the insulating membrane and with an electron beam of 10 keV/5 nA. For Auger mapping (i.e., elemental 2D distribution image), the CAE mode (constant analyser energy) corresponding to a fixed energy resolution was used.

3. Results and discussion

3.1. Electrochemical performance

Fig. 1a presents a digital image of the proprietary freestanding PVDF-HFP-based polymer electrolyte, having a lithium ionic conductivity

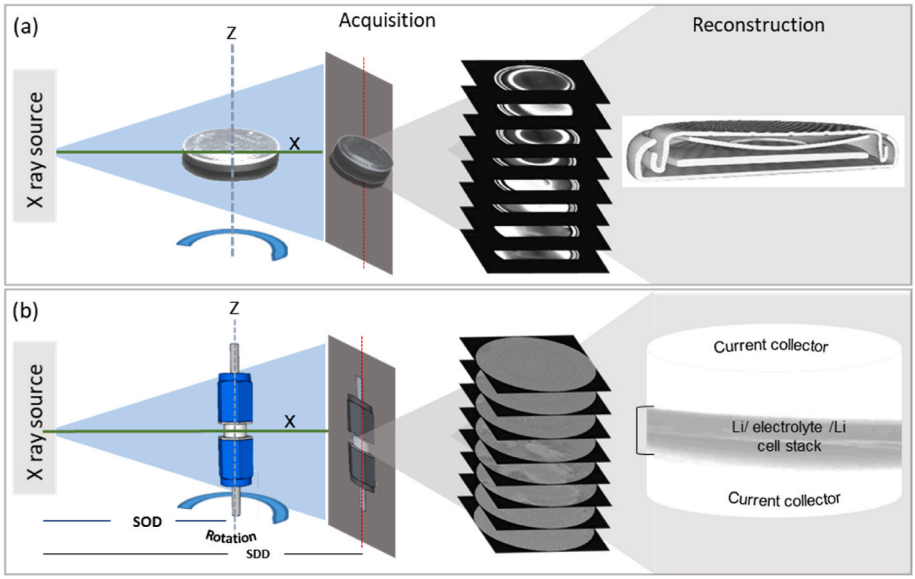

Fig. 2. Schematic X-ray tomography workflow for a Li/Li symmetric stack within (a) a coin cell casing and (b) a PFA Swagelok fitting.

above 10^{-3} S/cm at 70 °C. In this work the solid polymer electrolyte will be addressed as SPE.

The Li/Li symmetric cell with SPE was mounted within a PFA-based Swagelok fitting and subjected to galvanostatic cycling. Fig. 1b presents a digital image of the cell stack before cycling, which is compared to Fig. 1c, which depicts the stack after cycling. The interface stability was assessed by plating and stripping Li metal in the symmetric cell at 70 °C. Fig. 1d presents the time-dependent voltage profile for the Li/Li symmetric cell. At each current density, successive cycles consisting of 30 min plating and 30 min stripping were performed for a total duration of 6 h. Then, the cell resistance was measured, as indicated in Fig. 1e, by impedance spectroscopy, after which the process was repeated at a higher current density until failure of the cell. At the end of the cycling, the cell was opened in a glove box, and a change in the physical appearance of the polymer electrolyte was observed, as evidenced by a colour alteration (Fig. 1c), indicating that certain reactions took place.

The total resistance of the pristine cell is found to be around 20 Ωcm^2. We can observe that the initial current density of 0.03 mA/cm^2 results in a stable cycle life with a relatively small rise in polarisation. A further increase in the current density is systematically accompanied by

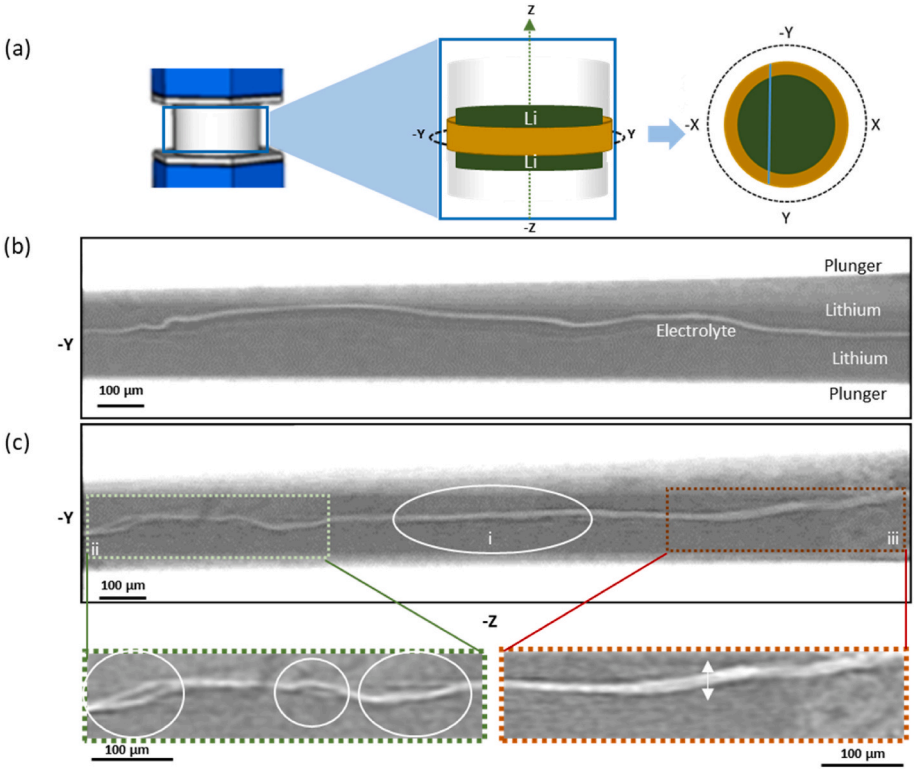

Fig. 3. (a) Schematic of symmetric cell within the Swagelok fitting. (b,c) 2D slice through the reconstructed 3D X-ray tomography datasets showing a selected cross-section (b) before and (c) after cycling (position corresponding to the blue line in the schematic presentation of the cell stack in (a)). (For interpretation of the references to colour in this figure legend, the reader is referred to the Web version of this article.)

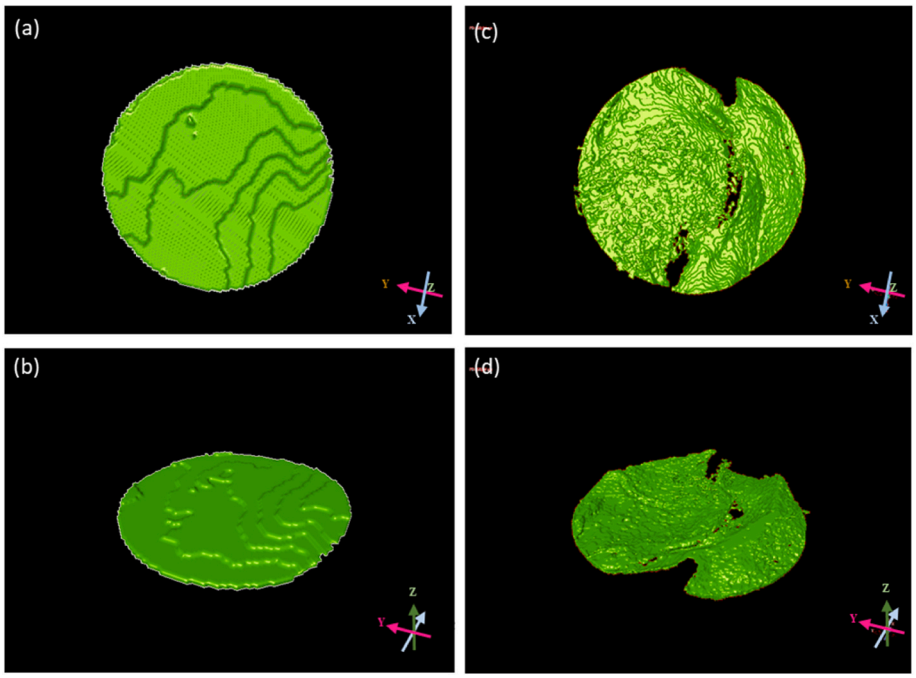

Fig. 4. 3D reconstruction of a region of interest (diameter ~500 μm) of the polymer electrolyte (a,*b*) before and (c,d) after cycling.

an increment in polarisation and therefore cell resistance, indicating issues with the interface [27–31]. At 0.32 mA/cm^2, for example, the cell presented a voltage of 48 mV and subsequently ascended to 57 mV following stripping and plating. The total increase in cell resistance is measured to be 160 Ωcm^2. The reduction in the resistance at the starting point of 0.36 mA/cm^2, accompanied by a disturbance of the voltage pattern, points to dendritic development. Total deterioration is observed at 0.42 mA/cm^2, as indicated by a significant voltage drop and decrease in resistance, most likely due to short-circuit from the Li dendrite growth [32,33].

The electrochemical performance of the symmetric cell offered a quick overview of the cell's interface behaviour with cycling, yet for a detailed understanding of the processes that took place, a finer analysis is required. We developed a generic framework for analysing the interface of the electrolyte used in this work. The framework consists in combining three advanced characterization techniques, namely screening with *in situ* laboratory X-ray tomography, and in-depth analysis with *ex situ* XPS and SEM/Auger analyses. The results obtained with these three techniques are reported in the next subsections.

3.2. *In situ laboratory X-ray tomography*

Visualization of the internal structures of the cell stack using *in situ/operando* analysis requires the use of an X-ray compatible cell holder. The term X-ray compatible implies that the holder itself should be as transparent to X-rays as possible (i.e. minimal thickness as well as low atomic number and density relative to the sample of interest), as such that the X-rays are principally probing the sample rather than the sample holder. To clarify this point, Fig. 2 compares a classical 2032-coin cell (~5 % transmission) with the PFA-based Swagelok fitting used in the current work (~34 % transmission). The schematic also illustrates the key principles behind X-ray tomography, including the rotation of the object of interest around an axis while simultaneously acquiring projections, followed by the reconstruction of a 3D volume. The 3D reconstruction obtained from the coin cell provides a good quality image of the stainless steel cell casing and the spring, yet yields hardly any contrast to analyse the cell stack itself (Fig. 2a). In contrast, the comparatively low X-ray attenuation of the PFA fitting renders it possible to visualize the cell stack (Fig. 2b). The steel current collectors appear very bright on the 3D reconstruction (just like the metal of the coin cell), and a further improvement of the cell would consist in replacing these by an electrically conductive yet low X-ray attenuating material such as carbon [34,35].

X-ray tomography was carried out to identify morphological changes of the cell, and to correlate them to the electrochemical observations. Fig. 3a represents a schematic of the symmetric cell within the Swagelok fitting. It also depicts the position and orientation of the vertical cross-section through the stack, shown in Fig. 3b and c. Brighter grey tones in the X-ray images correspond to denser and heavier phases [36–39]. The polymer electrolyte therefore, appears brighter in these images than the metallic lithium strips above and below it. Gaps would appear dark grey or black.

Fig. 3b shows 2D cross-section through the 3D reconstructed volume of the Li/Li symmetric cell before cycling. The electrolyte is in pristine condition with a constant thickness throughout. The absence of dark regions indicates proper contact with metallic lithium, which is in agreement with the electrochemical impedance measurement shown previously. The tomographic data also reveal that the electrolyte is not flat and that the thickness of the metallic strips is variable. This is a consequence of manual cell stack preparation. Note however that the entire cell stack is only around 300 μm in thickness and that the deviation of the real electrolyte position from the central plane nowhere exceeds ±80 μm.

Once the cell failed, after cycling for 118 h, a second tomography was taken in order to examine the morphological changes induced by the stripping-plating (Fig. 3c). Comparison with the pristine state shows that the electrolyte is displaced and deformed. Note that we are not the first to observe such relatively large displacements after periodic lithium stripping and plating, see e.g. Ref. [40]. Closer inspection reveals several other features. One can observe the presence of thin dark lines at several locations (i) along the electrolyte-lithium interface. This is consistent with contact loss and contributes to the observed voltage window enhancement during cycling. At some locations (ii), the electrolyte got separated and punctured. This allows for contact between the two metallic lithium strips and is coherent with cell shorting by Li dendrites. At other locations (iii), the electrolyte thickness increased around 47 %,

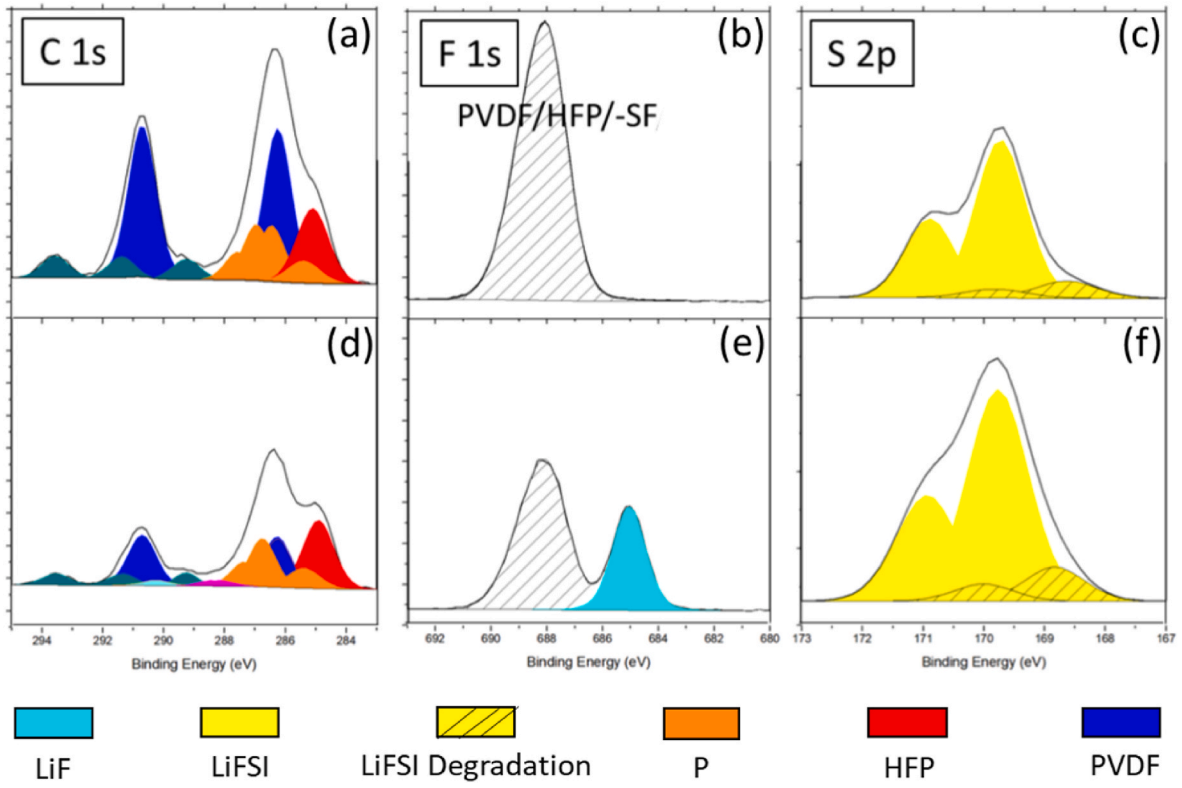

Fig. 5. Comparison of the C 1s, F 1s, and S 2p core XPS spectra before cycling (a–c) and after cycling (d–f) showing the evolution of the elements at Li/polymer interface with cycling performances.

which might be due to interphase layer formation from polymer membrane degradation during cycling [41,42].

While the tomogram reveals several interesting features, it is also clear that the selected voxel size of 4μm/voxel limits the quantification of those features. An advantage of laboratory-based X-ray tomography is that it enables performing higher resolution imaging of specific regions of interest in the data. While sub-micron resolution images can be acquired, such scans also take longer and lead to a higher radiation dose absorbed by the sample. Here, we illustrate the effect of doubling the resolution, and we focus on the region where a puncture in the electrolyte was observed in the 4μm/voxel dataset.

Fig. 4 (a,b) corresponds to a zoom on the electrolyte prior to cycling and (c,d) to a 2μm/voxel scan of the same region after cycling. The visualization uses false-colour to highlight the texture of the membrane. An animated sequence is provided as supplementary material (Fig. S1). Cross comparing Fig. 4 (a,b) and Fig. 4 (c,d) confirms the findings cited above: the initially pristine electrolyte became heavily deformed during cycling until the point it was punctured and the cell was shorted by Li dendrites. The added detail by doubling the resolution is also evident.

While X-ray tomography does give an indication of possible interphase layer formation via the thickness increase, it does not provide compositional information to support this hypothesis. Therefore, complementary *ex situ* XPS studies were performed.

3.3. *Ex situ XPS analysis*

After opening the cycled cell, an XPS analysis was carried out to compare the composition of the Li/SPE interface with the composition of the pristine polymer electrolyte membrane. As explained in Section 2.1, the SPE membrane consists of PVDF-HFP, plasticizers (hereafter noted P) and a lithium salt, LiFSI.

Fig. 5(a–c) shows C 1s, F 1s, and S 2p and core peaks of the component elements. Table S1 shows the atomic percentages (at. %) and binding energy (position in eV) associated with the chemical environments. The C 1s core peak has many components, including two major ones, located at 286.4 eV and 290.9 eV, corresponding to the chemical environments $–CH_2$ and $–CF_2$ present in the PVDF unit of the membrane. There are also three other components located at 286.4 eV, 291.5 eV and 293.7 eV attributed respectively to the –CF, $–CF_2$ and $–CF_3$ bonds present in the HFP unit of the membrane [25,26]. Other C 1s peaks are attributed to plasticizers, amongst others. For the F 1s core peak, a complex component located at 688.1 eV is attributed to $–CF_2$, $–CF_3$ and –SF present in the PVDF-HFP motif and in LiFSI. Finally, the S 2p core peak shows a doubling leading to S 2p components at 170.1 eV and 171.3 eV respectively, attributed to NSO_2F.

Fig. 5(d–f) shows XPS spectra after cycling, at the Li/SPE interface. There is a decrease in the intensity of the peaks from the PVDF-HFP identified by quantification before (58.3 at. %) and after (21.6 at. %) cycling (Table S1). This decrease indicates membrane covering by new species. An increase in the intensities of the core peaks attributed to the LiFSI chemical environment was also observed. The amount of LiFSI increases from 17.7 at. % to 27.1 at. % after cycling, indicating an accumulation of salt at the interface. There was also a decrease in the intensity of C 1s core peaks from the plasticizers, corresponding to 12.4 at. % compared with 15.1 at. % initially. We note the appearance of new components on the Li 1s core peak, located at 55.6 eV (not shown here) and on the F 1s core peak, located at 685.1 eV, characteristic of LiF induced by the degradation of the LiFSI salt during cycling (before cycling 0 at. %, after cycling 18.4 at.%). This LiF formation is accompanied by the formation of other organic compounds (not described here) that result from the degradation P and the lithium salt. XPS analysis therefore provides insight into the alteration of the Li/SPE interface incurred during galvanostatic cycling. The PVDF-HFP of the SPE membrane was found to be covered, due to the accumulation of LiFSI lithium salt, lithium fluoride and other organic compounds resulting from the degradation of constituents of the electrolyte membrane during cycling. Therefore, XPS approach in this work could identify and comprehend the causes of the observed thickness increment

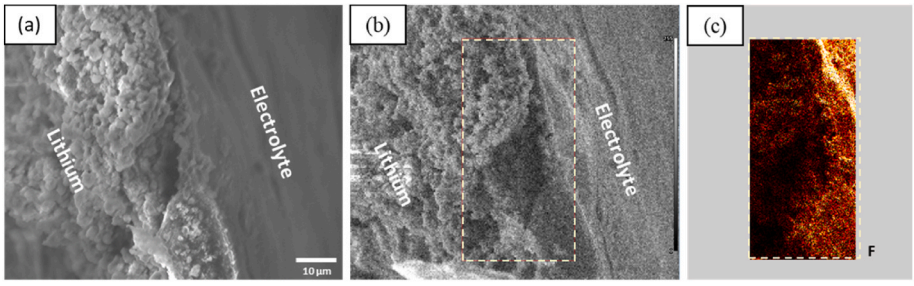

Fig. 6. (a) Cross-section SEM image of the interface between the polymer electrolyte and metallic lithium after cell cycling, (b) Auger image and (c) the corresponding map of F.

of the electrolyte after cycle, as evidenced in Fig. 3c (iii).

3.4. Ex situ SEM and auger analysis

The Li/SPE interface was further investigated using SEM and Auger mapping after cycling. These investigations supplement our earlier analysis by providing high-resolution and enlarged microstructural features of the interface. Cross-section SEM image Fig. 6a shows the microstructural features near the interface and confirms the presence of a microscopic gap and loss of contact between electrolyte and metallic lithium, as seen in the X-ray computed tomography data. Auger mapping of the same region (Fig. 6b) reveals the presence of F near the interface (Fig. 6c). This may be due to LiF formation and LiFSI accumulation at the Li/SPE interface during cycling. Both hypotheses are in accordance with the XPS results and X-ray tomography data.

4. Conclusion

In the present work, different approaches were used to characterize the degradation of a solid polymer electrolyte in a Li/Li symmetric cell during high-temperature cycling. We showed that *in situ* X-ray tomography is a reliable characterization approach that enabled identifying morphological changes in the cell stack, corresponding to interphase layer formation, membrane separation/puncture and loss of contact, despite its limited resolution.

These observations are highly supported by post-mortem *ex situ* studies with XPS, SEM, and Auger. The study provides a detailed description of multiple deterioration factors associated with cell failure, such as electrolyte degradation products and salt accumulation at the interface between the polymer-based membrane and the lithium, allowing future researchers to focus on these areas in order to improve cell performance and achieve optimal results.

As X-ray tomography is a non-invasive technique, it is compatible with *in operando* studies. Furthermore, laboratory X-ray tomographs are commonly encountered in research laboratories worldwide and therefore easier to access than synchrotron facilities. In light of our results, it follows that X-ray tomography could perform a key role in the development of polymer-based solid-state batteries by pinpointing the areas that are of interest to perform detailed analytical studies. Moreover, there is no immediately identifiable roadblock to apply the same methodology to study both anodes and cathodes, with both liquid and solid electrolytes, and contribute to the development of tomorrow's energy storage systems.

CRediT authorship contribution statement

Srabani Patra: Methodology, Investigation, Data curation, Visualization, Writing – original draft. **Julien Morey:** Investigation. **Lénaïc Madec:** Investigation, Supervision, Writing – review & editing. **Peter Moonen:** Writing – review & editing, Validation, Supervision, Project administration, Methodology, Investigation, Conceptualization.

Declaration of competing interest

The authors declare that they have no known competing financial interests or personal relationships that could have appeared to influence the work reported in this paper.

Data availability

Data will be made available on request.

Acknowledgement

The project RAISE2024 leading to this publication has received funding from the Excellence Initiative of the Université de Pau et des Pays de l'Adour – I-SITE E2S UPPA, a French "Investissements d'Avenir" programme (PIA2). The authors also thank TotalEnergies for providing DMEX with the Zeiss Xradia tomograph used in this work.

Appendix A. Supplementary data

Supplementary data to this article can be found online at https://doi.org/10.1016/j.jpowsour.2024.234506.

References

[1] M. Armand, J.M. Tarascon, Building better batteries, nature 451 (7179) (2008) 652–657.
[2] C. Fang, X. Wang, Y.S. Meng, Key issues hindering a practical lithium-metal anode, Trends in Chemistry 1 (2) (2019) 152–158.
[3] S. Randau, D.A. Weber, O. Kötz, R. Koerver, P. Braun, A. Weber, E. Ivers-Tiffée, T. Adermann, J. Kulisch, W.G. Zeier, F.H. Richter, Benchmarking the performance of all-solid-state lithium batteries, Nat. Energy 5 (3) (2020) 259–270.
[4] D. Zhou, D. Shanmukaraj, A. Tkacheva, M. Armand, G. Wang, Polymer electrolytes for lithium-based batteries: advances and prospects, Chem 5 (9) (2019) 2326–2352.
[5] A. Manthiram, X. Yu, S. Wang, Lithium battery chemistries enabled by solid-state electrolytes, Nat. Rev. Mater. 2 (4) (2017) 1–16.
[6] W. Xu, J. Wang, F. Ding, X. Chen, E. Nasybulin, Y. Zhang, J.G. Zhang, Lithium metal anodes for rechargeable batteries, Energy Environ. Sci. 7 (2) (2014) 513–537.
[7] K. Karthik, R. Murugan, Flexible high Li^+ conductive lithium garnet–based dry solid polymer electrolyte membrane with enhanced electrochemical performance for lithium metal batteries, Ionics 25 (2019) 4703–4711.
[8] L. Long, S. Wang, M. Xiao, Y. Meng, Polymer electrolytes for lithium polymer batteries, J. Mater. Chem. A 4 (26) (2016) 10038–10069.
[9] W. Tang, S. Tang, C. Zhang, Q. Ma, Q. Xiang, Y.W. Yang, J. Luo, Simultaneously enhancing the thermal stability, mechanical modulus, and electrochemical performance of solid polymer electrolytes by incorporating 2D sheets, Adv. Energy Mater. 8 (24) (2018) 1800866.
[10] J. Wan, J. Xie, X. Kong, Z. Liu, K. Liu, F. Shi, A. Pei, H. Chen, W. Chen, J. Chen, X. Zhang, Ultrathin, flexible, solid polymer composite electrolyte enabled with aligned nanoporous host for lithium batteries, Nat. Nanotechnol. 14 (7) (2019) 705–711.
[11] G. Feuillade, P. Perche, Ion-conductive macromolecular gels and membranes for solid lithium cells, J. Appl. Electrochem. 5 (1975) 63–69.
[12] T.J. Benedict, S. Banumathi, A. Veluchamy, R. Gangadharan, A.Z. Ahamad, S. Rajendran, Characterization of plasticized solid polymer electrolyte by XRD and AC impedance methods, J. Power Sources 75 (1) (1998) 171–174.

[13] I. López, J. Morey, J.B. Ledeuil, L. Madec, H. Martinez, A critical discussion on the analysis of buried interfaces in Li solid-state batteries. Ex situ and in situ/operando studies, J. Mater. Chem. A 9 (45) (2021) 25341–25368.
[14] L. Madec, J.B. Ledeuil, J. Morey, H. Martinez, Cross-section nano-Auger/SEM analysis to reveal bulk chemical/morphological properties of composites for energy storage, Electrochim. Acta 448 (2023) 142185.
[15] S.M. Bak, Z. Shadike, R. Lin, X. Yu, X.Q. Yang, In situ/operando synchrotron-based X-ray techniques for lithium-ion battery research, NPG Asia Mater. 10 (7) (2018) 563–580.
[16] J. Tippens, J.C. Miers, A. Afshar, J.A. Lewis, F.J.Q. Cortes, H. Qiao, T.S. Marchese, C.V. Di Leo, C. Saldana, M.T. McDowell, Visualizing chemomechanical degradation of a solid-state battery electrolyte, ACS Energy Lett. 4 (6) (2019) 1475–1483.
[17] G. Tonin, G.B. Vaughan, R. Bouchet, F. Alloin, M. Di Michiel, C. Barchasz, Operando investigation of the lithium/sulfur battery system by coupled X-ray absorption tomography and X-ray diffraction computed tomography, J. Power Sources 468 (2020) 228287.
[18] F. Shen, M.B. Dixit, X. Xiao, K.B. Hatzell, Effect of pore connectivity on Li dendrite propagation within LLZO electrolytes observed with synchrotron X-ray tomography, ACS Energy Lett. 3 (4) (2018) 1056–1061.
[19] W. Zhang, D. Schröder, T. Arlt, I. Manke, R. Koerver, R. Pinedo, D.A. Weber, J. Sann, W.G. Zeier, J. Janek, Electro) chemical expansion during cycling: monitoring the pressure changes in operating solid-state lithium batteries, J. Mater. Chem. A 5 (20) (2017) 9929–9936.
[20] P. Pietsch, V. Wood, X-ray tomography for lithium ion battery research: a practical guide, Annu. Rev. Mater. Res. 47 (2017) 451–479.
[21] T. Jousseaume, J.F. Colin, M. Chandesris, S. Lyonnard, S. Tardif, How beam damage can skew synchrotron operando studies of batteries, ACS Energy Lett. 8 (2023) 3323–3329.
[22] M. Li, W. Liu, D. Luo, Z. Chen, K. Amine, J. Lu, Evidence of morphological change in sulfur cathodes upon irradiation by synchrotron X-rays, ACS Energy Lett. 7 (2) (2022) 577–582.
[23] E.N. Antonio, M.F. Toney, Why it is important to determine and report the impact of probe radiation, Joule 6 (4) (2022) 723–725.
[24] K.K. Neelisetty, X. Mu, S. Gutsch, A. Vahl, A. Molinari, F. Von Seggern, M. Hansen, T. Scherer, M. Zacharias, L. Kienle, V.K. Chakravadhanula, Electron beam effects on oxide thin films—structure and electrical property correlations, Microsc. Microanal. 25 (3) (2019) 592–600.
[25] K.N. Wood, G. Teeter, XPS on Li-battery-related compounds: analysis of inorganic SEI phases and a methodology for charge correction, ACS Appl. Energy Mater. 1 (9) (2018) 4493–4504.
[26] L. Caracciolo, L. Madec, H. Martinez, XPS analysis of K-based reference compounds to allow reliable studies of solid electrolyte interphase in K-ion batteries, ACS Appl. Energy Mater. 4 (10) (2021) 11693–11699.
[27] Y. Lu, C.Z. Zhao, H. Yuan, X.B. Cheng, J.Q. Huang, Q. Zhang, Critical current density in solid-state lithium metal batteries: mechanism, influences, and strategies, Adv. Funct. Mater. 31 (18) (2021) 2009925.
[28] S. Patra, J. Narayanasamy, S. Chakravarty, R. Murugan, Higher critical current density in lithium garnets at room temperature by incorporation of an Li_4SiO_4-related glassy phase and hot isostatic pressing, ACS Appl. Energy Mater. 3 (3) (2020) 2737–2743.
[29] Q. Li, H.Y. Sun, Y. Takeda, N. Imanishi, J. Yang, O. Yamamoto, Interface properties between a lithium metal electrode and a poly (ethylene oxide) based composite polymer electrolyte, J. Power Sources 94 (2) (2001) 201–205.
[30] M. Rosso, T. Gobron, C. Brissot, J.N. Chazalviel, S. Lascaud, Onset of dendritic growth in lithium/polymer cells, J. Power Sources 97 (2001) 804–806.
[31] Y. Sun, J. Wang, D. Fu, F. Zhang, Z. Wang, X. Chen, J. Xu, J. Hu, X. Wu, Flexible composite solid electrolyte with an active inorganic filler, ACS Sustain. Chem. Eng. 9 (5) (2021) 2237–2245.
[32] M.D. Berliner, B.C. McGill, M. Majeed, D.T. Hallinan, Electrochemical kinetics of lithium plating and stripping in solid polymer electrolytes: pulsed voltammetry, J. Electrochem. Soc. 166 (2) (2019) A297.
[33] D.M. Pesko, Z. Feng, S. Sawhney, J. Newman, V. Srinivasan, N.P. Balsara, Comparing cycling characteristics of symmetric lithium-polymer-lithium cells with theoretical predictions, J. Electrochem. Soc. 165 (13) (2018) A3186.
[34] E.A. Zwanenburg, M.A. Williams, J.M. Warnett, Review of high-speed imaging with lab-based x-ray computed tomography, Meas. Sci. Technol. 33 (1) (2021) 012003.
[35] O.J. Borkiewicz, B. Shyam, K.M. Wiaderek, C. Kurtz, P.J. Chupas, K.W. Chapman, The AMPIX electrochemical cell: a versatile apparatus for in situ X-ray scattering and spectroscopic measurements, J. Appl. Crystallogr. 45 (6) (2012) 1261–1269.
[36] J. Scharf, M. Chouchane, D.P. Finegan, B. Lu, C. Redquest, M.C. Kim, W. Yao, A. A. Franco, D. Gostovic, Z. Liu, M. Riccio, Bridging nano-and microscale X-ray tomography for battery research by leveraging artificial intelligence, Nat. Nanotechnol. 17 (5) (2022) 446–459.
[37] J. Banhart (Ed.), Advanced Tomographic Methods in Materials Research and Engineering, vol. 66, OUP Oxford, 2008.
[38] X. Lu, A. Bertei, D.P. Finegan, C. Tan, S.R. Daemi, J.S. Weaving, K.B. O'Regan, T. M. Heenan, G. Hinds, E. Kendrick, D.J. Brett, 3D microstructure design of lithium-ion battery electrodes assisted by X-ray nano-computed tomography and modelling, Nat. Commun. 11 (1) (2020) 2079.
[39] D.P. Finegan, S.J. Cooper, B. Tjaden, O.O. Taiwo, J. Gelb, G. Hinds, D.J. Brett, P. R. Shearing, Characterising the structural properties of polymer separators for lithium-ion batteries in 3D using phase contrast X-ray microscopy, J. Power Sources 333 (2016) 184–192.
[40] Sun Fu, Xin He, Xiaoyu Jiang, Markus Osenberg, Jie Li, Zhou Dong, Kang Dong, André Hilger, Xiaoming Zhu, Rui Gao, Xiangfeng Liu, Kai Huang, De Ning, Henning Markötter, Li Zhang, Fabian Wilde, Yuliang Cao, Martin Winter, Ingo Manke, Advancing knowledge of electrochemically generated lithium microstructure and performance decay of lithium ion battery by synchrotron X-ray tomography, Mater. Today 27 (2019) 21–32.
[41] E. Peled, S. Menkin, SEI: past, present and future, J. Electrochem. Soc. 164 (7) (2017) A1703.
[42] C. Xu, B. Sun, T. Gustafsson, K. Edström, D. Brandell, M. Hahlin, Interface layer formation in solid polymer electrolyte lithium batteries: an XPS study, J. Mater. Chem. A 2 (20) (2014) 7256–7264.